sciendo

Civil and Environmental Engineering
Vol. 19, Issue 1, 391-405, DOI: 10.2478/cee-2023-0035

THE EFFECT OF ROTATION RATE PARAMETER ON TWO CIRCULAR CYLINDERS IN STEADY AND UNSTEADY REGIMES AT DIFFERENT REYNOLDS NUMBERS

M. ESSAHRAOUI[1, *], R. EL BOUAYADI[1], A. SAAD[1]

[1] ASELAB, Advanced Systems Engineering Laboratory, National School of Applied Sciences, Ibn Tofail University, Kenitra, Morocco.
[*] corresponding author: saad_aouatif@yahoo.fr, marouane.essahraoui@uit.ac.ma

Abstract

The effect of rotation rate parameter, cylinder diameter, and the variation of Reynolds number on the circular cylinder was the main object of this 2D numerical study. Rotating and stationary circular cylinder in steady and unsteady incompressible flow has been analysed. For each value of Reynolds number, we have varied the rotation rate parameter clockwise and anti-clockwise to visualize their effect on the drag, lift, and coefficients. All cases have carried out steady laminar, unsteady laminar, and turbulent regimes. A realizable K-epsilon model has been used to solve the Navier Stokes equations for the turbulent regime. Results were in good agreement with the recent findings.

Keywords:

Steady;
Unsteady;
Turbulent;
Rotation rates;
Laminar.

1 Introduction

Fluid flow around bluff bodies has attracted much attention in the literature because of its practical importance in engineering design. Thus, the applications on bluff bodies could help engineers avoid structural damage that fluid flow would cause in several fields (large buildings, monuments, and towers that have been exposed permanently to the wind).

A circular cylinder is one of the bluffest bodies that could help researchers understand the influence phenomenon around a wide range of applications that can be modelled as a cylinder (pipelines, heat exchanger, etc.). At a low Reynolds number in the range of $0 \leq \mathrm{Re} \leq 6$ [22], the fluid moves from left to right in a steady-state, and the flow fields are symmetrical upstream and downstream of the cylinder. Otherwise, in a range of $10 \leq \mathrm{Re} \leq 40$, an increase in Reynolds number breaks up the symmetry of the fluid flow around the cylinder and lets us visualize two attached eddies in the flow behind the cylinder where these two recirculation regions are growing if we increase the Reynolds number. The sudden transition from steady to oscillating is called a supercritical Hopf bifurcation. Sreenivasan [17] have established experiments, where they have estimated that this transition occurs at Reynolds number of around $\mathrm{Re} = 46$. When the value of Reynolds number surpasses the subcritical value, the vortex shedding appears and oscillates periodically behind the cylinder until a value of turbulent regime where the Reynolds number is higher than $\mathrm{Re} > 300$ [12, 14].

Based on several kinds of literature sources, we have investigated the effect of the rotation rate parameter on the circular cylinder in the case of stationary where $\alpha = 0$, and in revolving case for $\alpha = -1, -0.5,\ 0.5 \text{ and } 1$. We concluded that the rotation rate parameter broke up the wake region's symmetry at low Reynolds number values, where these results have been confirmed by [8]. Kang [11] have demonstrated that at specific values of $0 \leq \alpha \leq 2.5$ for $\mathrm{Re} < 40$, the flow stays stable and doesn't provide any vortex. Ingham [10] has reproduced the same experience at $\mathrm{Re} < 40$ for $\alpha \leq 0.5$ and he has provided the findings of [11]. Otherwise, the rotation rate significantly affects the lift and drag coefficients. Tokumaru [20] have demonstrated through laboratory experiments that the oscillatory cylinder rotation could help achieve a significant control of the fluid dynamics in the wake. The rotating cylinders also have affected the lift and drag coefficients. At each rotation rate value, we will obtain

© Author(s) 2023. This work is distributed under the Creative Commons BY 4.0 license (https://creativecommons.org/licenses/by/4.0/).

negative and positive values of drag and lift, respectively, and Prandtl [13] was one of the earliest who has applied this technique to the circular cylinder. As a result of his research, he has found that the maximum lift in a uniform flow was approximately 12.6. Tokumaru [20] have investigated how the steadily rotating cylinder and the addition of forced rotary oscillations affect the lift coefficients. The value of the lift coefficient increased with an expansion of the forced oscillating. Badr, Coutanceau, Dennis, and Menard [2] have developed an experimental and theoretical study of unsteady flow past a rotating cylinder for high Reynolds numbers in a range of $10^3 \leq \mathrm{Re} \leq 10^4$ at speed ratios between 0.5 and 3, they have studied the effect of the rotating cylinder on the vortex generated behind the cylinder and compared each path of the vortex structures by the increase in speed ratio values. The lift and drag variation have also been investigated for three rotation rates $\alpha = 0.5, 1, 3$ at different periods τ.

The capacity of computers is still one of the greatest obstacles preventing researchers from determining which computational fluid domain might affect the precision of the results. Tezduyar and Sihih [19] investigated how downstream placement in the fluid domain influences the unsteady compressible flow at Re = 100. They attempted to ascertain how far downstream could be to avoid inconsistencies in results, and have identified the downstream at a distance of 25 diameters from the center of the cylinder, but the second example has been located at a distance of only 2.5 diameters from the center of the cylinder. Behr, Hastreiter, Mittal, and Tezduyar [4] have justified the critical impact of lateral boundaries of the computational fluid domain on the global parameters at Re = 100. They conclude that the distance between the lateral edges and the cylinder should be eight diameters from the cylinder center.

In this work, a 2D numerical study shall investigate stationary and rotating cylinders immersed in a uniform stream for steady and unsteady flow regime from low to high values of Reynolds number at rotation rates in a range of $\alpha = -1, -0{,}5, 0.5, 0 \text{ and } 1$. At the same time, a steady laminar study has been investigated for $\mathrm{Re} = 5, 20, 40$ at rotation rates in a range of $\alpha = -1, -0{,}5, 0.5, 0 \text{ and } 1$, and an unsteady laminar study for $\mathrm{Re} = 60, 150$ at the same values of rotation rates. Similarly, for a turbulent regime, the study has been undertaken for Re = 1000 and 3900. The variation of drag and lift coefficients has been investigated in CCW (counter-clockwise) and CW (clockwise) rotation at different Reynolds number for various diameters $(D_1 = 100\ \mathrm{mm},\ D_2 = 300\ \mathrm{mm})$. Two separate radii were chosen because the rotation of a cylinder in a fluid produces a complex flow pattern that impacts fluid properties such as streamlines, vortex shedding, pressure contours, and velocity contours. The objective of the study was to examine the effect of cylinder size on these flow characteristics and determine whether it had a significant impact.

2 Numerical methods

2.1 Physical domain

Simulation of flow around both stationary and rotating cylinders has been established in sizeable computational domain. We have set the upstream and downstream 11.5*D* and 20*D*, respectively, away from the center of the cylinder and the lateral boundaries 12.5*D* away from the center of the cylinder. Following the study of [6], who have demonstrated that for better results, we must set lateral boundaries away at least eight diameters from the center of the cylinder. Selection of the computational domain is one of the main concerns facing all researchers where discrepancies in the results appear in an unstable regime. The cylinder rotates by the non-dimensional α parameter, defined as $\alpha = \omega D/2U_\infty$ where is ω the angular rotational speed, D is the diameter of the cylinder, and U_∞ is the uniform velocity from the inlet. The boundary conditions that have been set include the following:

The inlet has a Dirichlet condition $(u = U_\infty, v = 0)$, with the velocity inlet U_∞ changing based on the Reynolds number and cylinder diameter for each case. The outlet, on the other hand, has a Neumann condition $\frac{\partial u}{\partial x} = 0$. Both cylinders are experiencing a no-slip condition, while the upper and lower boundaries have a no-penetration condition. Lastly, the outlet has a pressure gradient of zero, and its pressure is set to $p = p_{out}$. According to [11], who have studied a sizeable computational domain, investigating the effect of computational domain dimensions on the accuracy of the results.

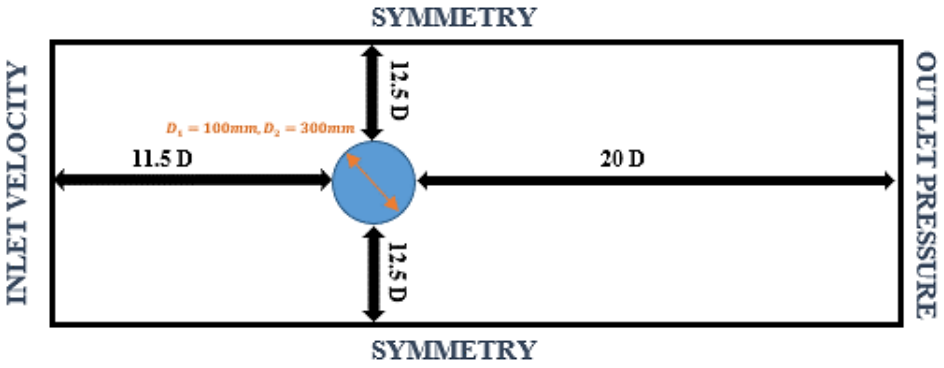


Fig. 1: Computational domain.

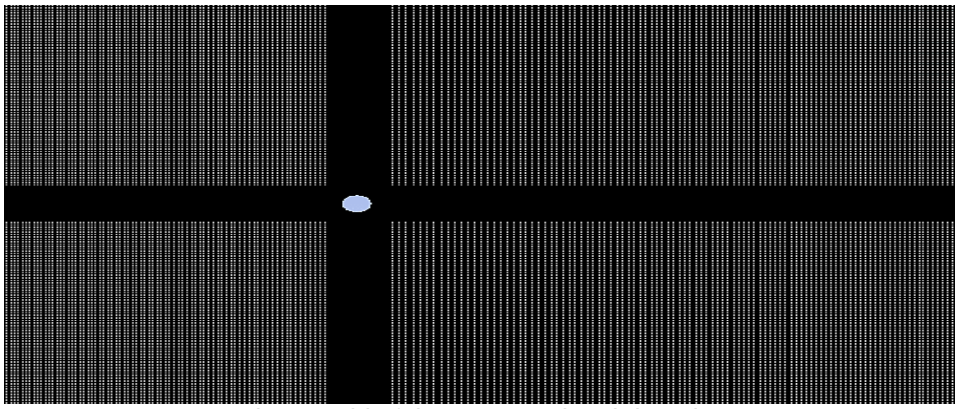


Fig. 2: Grid of the computational domain.

The grid does not have a consistent distribution throughout. In order to discretize the computational domain, the hyperbolic tangent function is put into practice. The cells that are located closest to the surface cylinders are stacked in layers, and their size increases in a predictable manner as one moves further away from the cylinder's edge. The y^+ value, which indicates the distance from the wall, is often quite near to 1 in most cases, which is an indication that the grid has been refined to a high degree. This study employed a total of $N = 624$ time steps for its analysis of unstable laminar and turbulent regimes, with the size of Δt (time steps) varying according to how the Reynolds number and the diameter of the cylinder changed for each scenario.

For both cylinders, the computational domain was divided into 113100 grid cells and 113910 nodes. In an effort to increase the accuracy of the CFD solver's findings, structured refined mesh has been applied around and downstream of the two cylinders, and the approach utilized for meshing is the rectangular domain with smooth quadrilateral grids [14].

2.2 Governing equations

Continuity and Navier Stokes equations (N-S equations) have been used for simulating the incompressible viscous flow. The equations below represents the continuity equation, the governing equations of unsteady flow, Reynold's stress tensor, turbulence kinetic energy k, and its dissipation rate ε, respectively.

$$\frac{\partial u_i}{\partial x_i} = 0 \ , \tag{1}$$

$$\frac{\partial u_i}{\partial t} + u_j \frac{\partial u_i}{\partial x_j} = -\frac{1}{\rho}\frac{\partial p}{\partial x_i} + \nu \frac{\partial^2 u_i}{\partial x_j^2} - \frac{\partial \overline{u_i' u_j'}}{\partial x_j} \ , \tag{2}$$

$$\overline{-\partial u_i' u_j'} = \nu_T \left(\frac{\partial u_i}{\partial x_j} + \frac{\partial u_j}{\partial x_i}\right) - \frac{2}{3} k \delta_{ij} \ , \tag{3}$$

$$\frac{\partial \rho k}{\partial t} + \frac{\partial \rho k u_i}{\partial x_i} = \frac{\partial}{\partial x_j}\left[\left(\mu + \frac{\mu_T}{\sigma_k}\right)\frac{\partial k}{\partial x_j}\right] + G_k - \rho\varepsilon \ , \tag{4}$$

$$\frac{\partial \rho \varepsilon}{\partial t} + \frac{\partial \rho \varepsilon u_i}{\partial x_i} = \frac{\partial}{\partial x_j}\left[\left(\mu + \frac{\mu_T}{\sigma_\varepsilon}\right)\frac{\partial \varepsilon}{\partial x_j}\right] + C_{1\varepsilon}\frac{\varepsilon}{k}(G_k) - C_{2\varepsilon}\rho\frac{\varepsilon^2}{k}\,. \quad (5)$$

For high Reynolds number, the k-epsilon model has been used to solve the instantaneous N-S equations [5]. We have used the k-epsilon model for both stationary and rotating cylinders, where k-epsilon can perfectly predict the flow behavior in such high values of Reynolds number. Drag and lift coefficients are the fundamental characteristic parameters of the fluid, which are defined as follows:

$$C_d = \frac{2F_d}{\rho U^2 A}\,, \quad (6)$$

$$C_l = \frac{2F_l}{\rho U^2 A}\,. \quad (7)$$

3 Results and discussion

Numerous experimental and numerical investigations have shown that when $\mathrm{Re} \leq 5$, the flow of fluid over a fixed cylinder is symmetrical in both the Y and X directions. In the range of $5 \leq \mathrm{Re} \leq 40$, the symmetry over the cylinder breaks, resulting in the formation of a pair of symmetrical vortices rotating in a clockwise and counter-clockwise direction in the wake just behind the cylinder. As the Reynolds number increases, these vortices separate, forming the well-known Kármán vortex street. However, an increase in Reynolds number to very high values can cause instabilities behind the cylinder, resulting in an alternating oscillation of the fluid flow. This study aims to determine the effect of rotation rates on both CW and CCW steady and unsteady flow regimes in a large computational fluid domain for two cylinder diameters D_1 = 100 mm, D_2 = 300 mm at various Reynolds numbers. A two-dimensional numerical study has been conducted to examine the impact of CW and CCW rotation rates on the lift and drag variations for each case, and then the behavior of pressure, velocity, and streamlines patterns around and along the wake of the cylinders will be visualized.

3.1 Steady state

3.1.1 Drag and lift coefficient variation

The drag and lift coefficients of a stationary and spinning cylinder with different diameters $D_1 = 100\ \mathrm{mm}$ & $D_2 = 300\ \mathrm{mm}$ under steady flow conditions are shown in Tables 1, 2, and 3, respectively. The results of the stationary cylinder were in good agreement with the experimental and numerical results given in [16] and [18], respectively. When Reynolds numbers increased, drag values decreased while the lift coefficient stayed unchanged due to the cylinder's symmetry and the formation of recirculation zones behind it. According to the study of [2], the drag coefficient of spinning cylinders dropped for both CCW and CW rotation speeds as the Reynolds number changed. At various Reynolds numbers $\mathrm{Re} = 5, 20, and\ 40$, the lift coefficient produced negative and positive values for CW and CCW rotational speeds, respectively. According to our observations, in a large computational fluid domain, the drag and lift coefficients remain the same for both CCW and CW rotations. In the case of $\mathrm{Re} = 40$, we also observed, as shown in Table 3, that the diameter adjustment has a considerable impact on the drag and lift coefficient values. Except for the instance represented in Table 3, we infer that rotation rate parameter and cylinder diameter have no significant influence on the coefficient values for drag and lift. The research has ramifications for fields such as fluid dynamics and mechanical engineering.

Table 1: Variation of drag and lift coefficients for different rotation rate at Re = 5.

	$\mathbf{Re = 5}$				
	$\boldsymbol{\alpha = -1}$	$\boldsymbol{\alpha = -0.5}$	$\boldsymbol{\alpha = 0}$	$\boldsymbol{\alpha = 0.5}$	$\boldsymbol{\alpha = 1}$
C_d for $D_1 = 100$ mm	0.9555	1.0109	1.0312	1.0109	0.9554
C_d for $D_2 = 300$ mm	0.9505	1.0122	1.0326	1.0121	0.9567
C_l for $D_1 = 100$ mm	0.4116	0.1766	0.0004	-0.1758	-0.4110
C_l for $D_2 = 300$ mm	0.4176	0.1755	-0.0004	-0.1764	-0.4112

Table 2: Variation of drag and lift coefficients for different rotation rate at Re = 20.

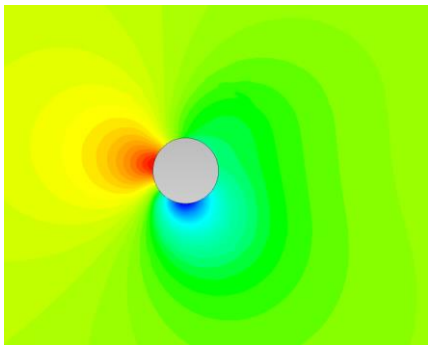
	$\mathbf{Re = 20}$				
	$\boldsymbol{\alpha = -1}$	$\boldsymbol{\alpha = -0.5}$	$\boldsymbol{\alpha = 0}$	$\boldsymbol{\alpha = 0.5}$	$\boldsymbol{\alpha = 1}$
C_d for $D_1 = 100$ mm	0.3922	0.4201	0.4298	0.4201	0.3921
C_d for $D_2 = 300$ mm	0.3923	0.4203	0.4301	0.4203	0.3951
C_l for $D_1 = 100$ mm	0.5453	0.2675	-0.0003	-0.2681	-0.5457
C_l for $D_2 = 300$ mm	0.5451	0.2681	0.0003	-0.2675	-0.5427

Table 3: Variation of drag and lift coefficients for different rotation rate at Re = 40.

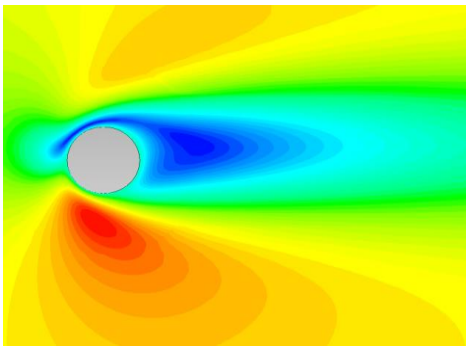
	$\mathbf{Re = 40}$				
	$\boldsymbol{\alpha = -1}$	$\boldsymbol{\alpha = -0.5}$	$\boldsymbol{\alpha = 0}$	$\boldsymbol{\alpha = 0.5}$	$\boldsymbol{\alpha = 1}$
C_d for $D_1 = 100$ mm	0.2700	0.2995	0.3104	0.2994	0.2700
C_d for $D_2 = 300$ mm	0.3923	0.4203	0.3109	0.4203	0.3951
C_l for $D_1 = 100$ mm	0.5179	0.2550	2.10E-05	-0.2551	-0.5179
C_l for $D_2 = 300$ mm	0.5451	0.2681	0.0003	-0.2675	-0.5427

3.1.2 Velocity and pressure contours

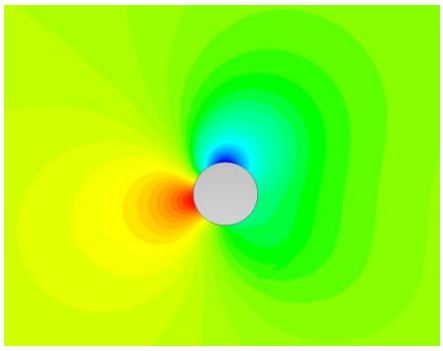
Flow stays symmetrical in a stationary circular cylinder with a Reynolds number of $\mathrm{Re} = 5$, but recirculation zones extend as the Reynolds number increases from $10 \leq \mathrm{Re} \leq 46$. A Reynolds number of 20 was used to evaluate the effect of rotation speeds on the flow. Fig. 3 and 4 illustrate the distribution of pressure and velocity throughout the cylinder surface and wake region for both CCW and CCW rotation rate. The investigation indicated that rotation rate significantly affected the flow, resulting in the movement of stagnation point on the upper and lower sides of the cylinder surface and the absence of vortices created behind the stationary cylinder. By eliminating the recirculation zone, rotating cylinders decreased drag and increased lift coefficient. The Magnus effect, which produced a positive lift in CCW direction and a negative lift in the CW direction, was seen for all values of alpha, with the pressure around the cylinder having the opposite sign. This could aid in our comprehension of the mechanisms governing the behavior of rotating cylinders.



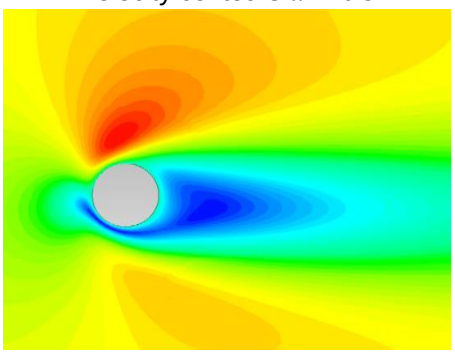
Pressure contours $\alpha = 0.5$



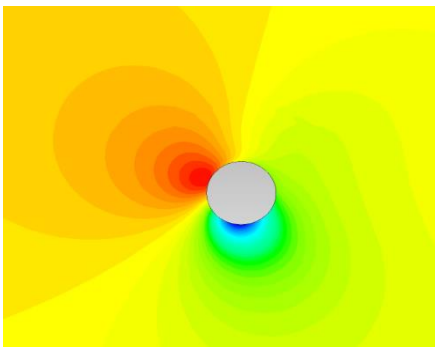
Velocity contours $\alpha = 0.5$



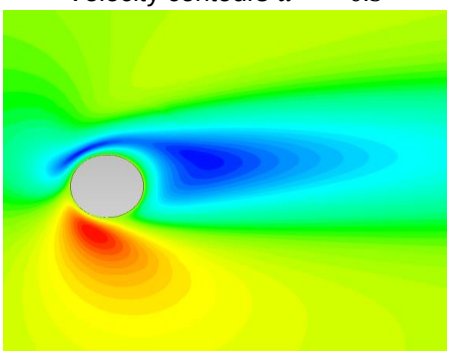
Pressure contours $\alpha = -0.5$



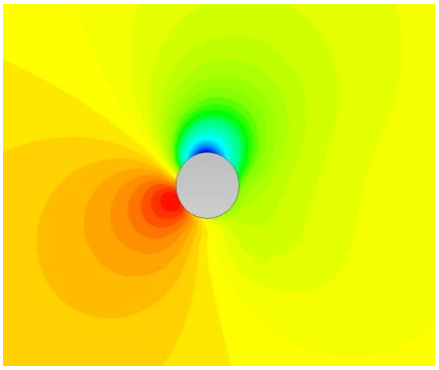
Velocity contours $\alpha = -0.5$



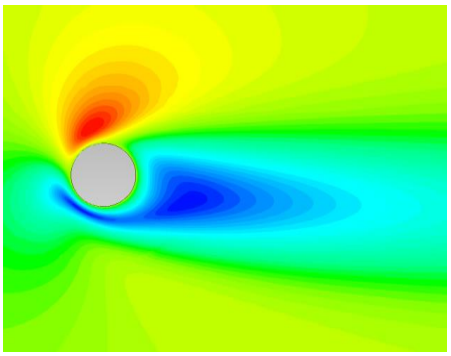
Pressure contours $\alpha = 1$



Velocity contours $\alpha = 1$

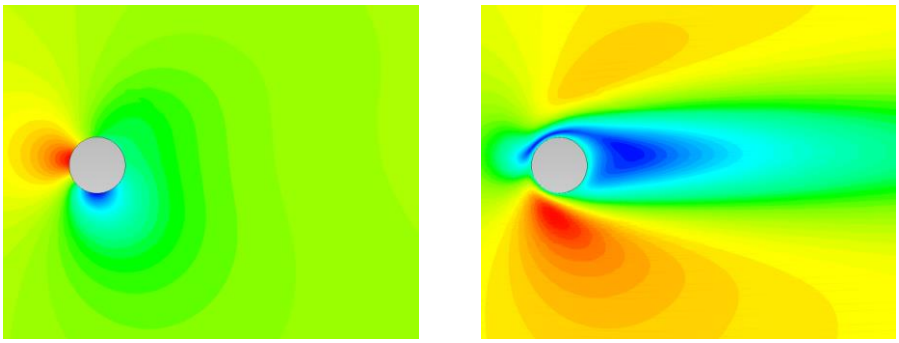


Pressure contours $\alpha = -1$

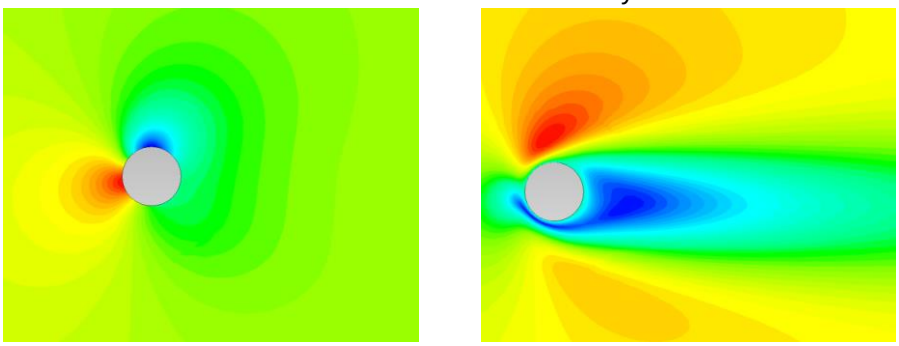


Velocity contours $\alpha = -1$

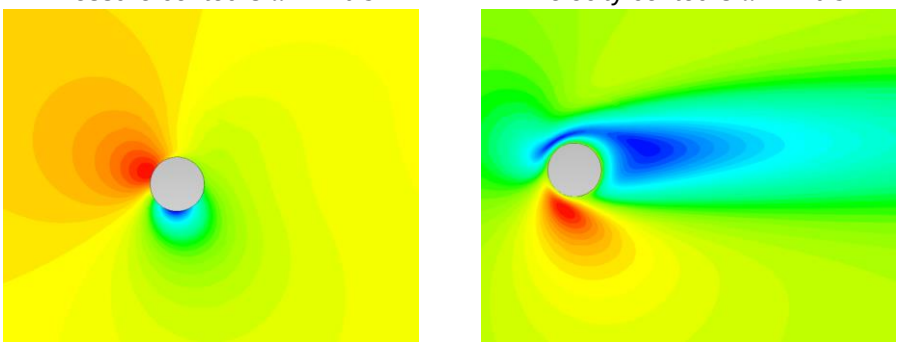
Fig. 3: Pressure and Velocity contours for $D_1 = 100$ mm at Re $= 20$.



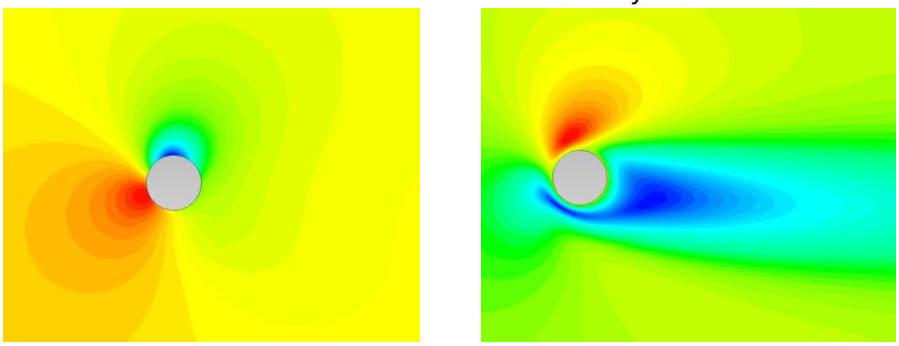
Pressure contours $\alpha = 0.5$ Velocity contours $\alpha = 0.5$



Pressure contours $\alpha = -0.5$ Velocity contours $\alpha = -0.5$



Pressure contours $\alpha = 1$ Velocity contours $\alpha = 1$



Pressure contours $\alpha = -1$ Velocity contours $\alpha = -1$

Fig 4: Pressure and Velocity contours for $D_1 = 300\text{mm}$ at $\text{Re} = 20$.

3.1.3 Streamlines patterns

Fig. 5 depicts the streamlines at $\text{Re} = 20$. for both diameters of cylinders. When $\alpha = 0$ we compared our results with [7] and [8]. Both CWW and CW spinning cylinders influence the streamline pattern near the surface cylinder for a variety of $\alpha = -1, -0.5, 0.5, 1$ values. We discovered that the effect of rotating CCW was comparable to that of rotating CW, and that the rotation parameters had the same influence on the streamline patterns regardless of the Reynolds numbers at steady state. This caused streamlines to sweep in the direction of the rotation rates, preventing flow separation from the surface of the cylinder. Our observations of the streamlined behavior of spinning cylinders were comparable to those from prior research [10].

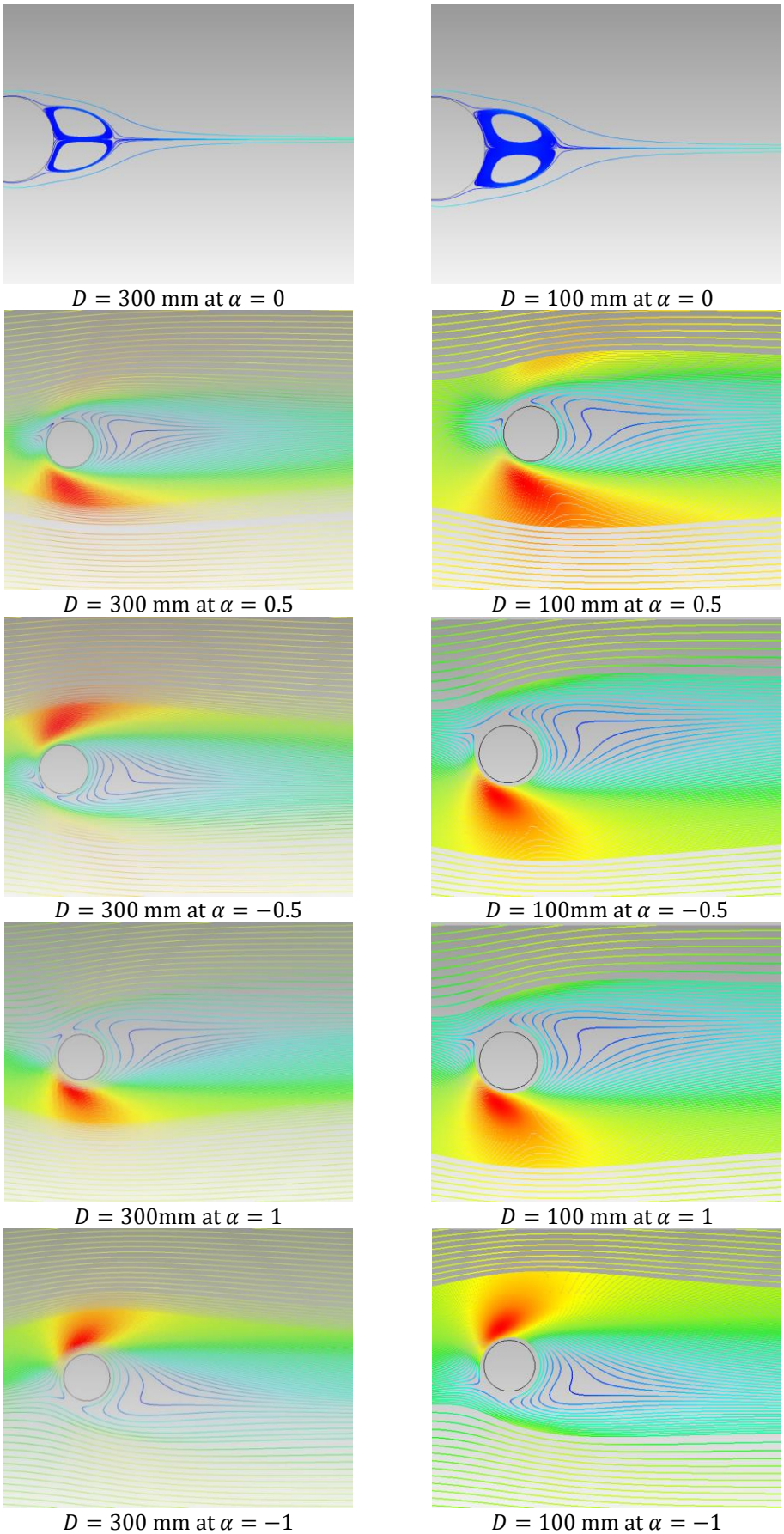


Fig. 5: Streamlines patterns at Re = 20.

3.2 Unsteady state

3.2.1 Drag and lift variation

We recalculated the coefficients of drag and lift for an unstable flow regime in order to see if the parameters of CCW and CW rotation may provide different results between steady and unsteady flow behind the circular cylinder. Considered were both turbulent and unstable laminar flows. Tables below illustrate the differences in drag and lift coefficients for stationary and rotating cylinders with $\mathrm{Re} = 60, 150, 1000, 3900$. The effects of CCW and CW rotation rate and cylinder diameter on drag and lift values are consistent with the steady-state regime. As α increases, drag coefficient decreases and lift coefficient increases.

Table 4: Variation of drag and lift coefficients for different rotation rate at Re = 60.

	$\mathbf{Re = 60}$				
	$\boldsymbol{\alpha = -1}$	$\boldsymbol{\alpha = -0.5}$	$\boldsymbol{\alpha = 0}$	$\boldsymbol{\alpha = 0.5}$	$\boldsymbol{\alpha = 1}$
C_d for $D_1 = 100$ mm	0.2271	0.2658	0.2676	0.2658	0.2271
C_d for $D_2 = 300$ mm	0.2271	0.2659	0.2703	0.2659	0.2385
C_l for $D_1 = 100$ mm	0.4878	0.2631	0.0113	-0.2630	-0.4880
C_l for $D_2 = 300$ mm	0.4887	0.2624	-0.0017	-0.2624	-0.4717

Table 5: Variation of drag and lift coefficients for different rotation rate at Re = 150.

	$\mathbf{Re = 150}$				
	$\boldsymbol{\alpha = -1}$	$\boldsymbol{\alpha = -0.5}$	$\boldsymbol{\alpha = 0}$	$\boldsymbol{\alpha = 0.5}$	$\boldsymbol{\alpha = 1}$
C_d for $D_1 = 100$ mm	0.2200	0.2420	0.2611	0.2420	0.2200
C_d for $D_2 = 300$ mm	0.2205	0.2419	0.2525	0.2421	0.2206
C_l for $D_1 = 100$ mm	0.3676	0.1370	0.0751	-0.1369	-0.3676
C_l for $D_2 = 300$ mm	0.3677	0.1366	-0.0331	-0.1366	-0.3679

Table 6: Variation of drag and lift coefficients for different rotation rate at Re = 1000.

	$\mathbf{Re = 1000}$				
	$\boldsymbol{\alpha = -1}$	$\boldsymbol{\alpha = -0.5}$	$\boldsymbol{\alpha = 0}$	$\boldsymbol{\alpha = 0.5}$	$\boldsymbol{\alpha = 1}$
C_d for $D_1 = 100$ mm	0.1815	0.1886	0.1994	0.1889	0.1815
C_d for $D_2 = 300$ mm	0.1812	0.1889	0.2004	0.1888	0.1814
C_l for $D_1 = 100$ mm	0.3625	0.1194	0.0177	-0.1185	-0.3642
C_l for $D_2 = 300$ mm	0.3658	0.1172	-0.0482	-0.1174	-0.3659

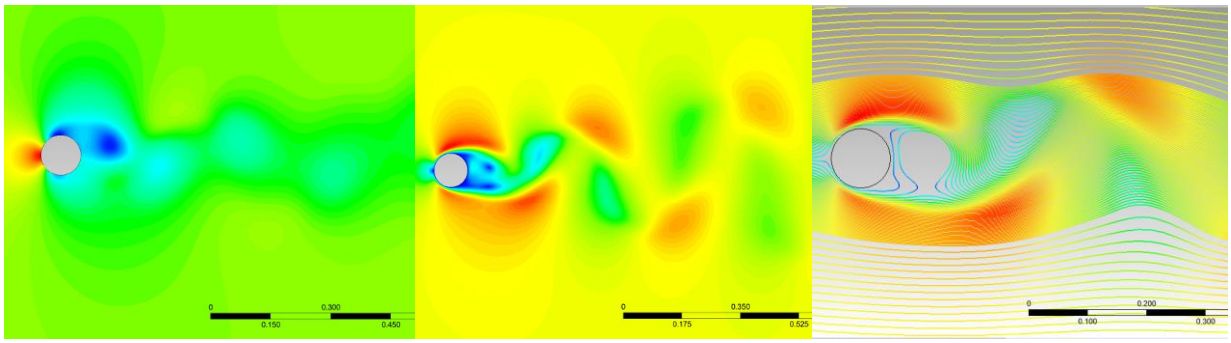
Table 7: Variation of drag and lift coefficients for different rotation rate at Re = 3900.

	$\mathbf{Re = 3900}$				
	$\boldsymbol{\alpha = -1}$	$\boldsymbol{\alpha = -0.5}$	$\boldsymbol{\alpha = 0}$	$\boldsymbol{\alpha = 0.5}$	$\boldsymbol{\alpha = 1}$
C_d for $D_1 = 100$ mm	0.1192	0.1568	0.1629	0.1566	0.1190
C_d for $D_2 = 300$ mm	0.1235	0.1560	0.1623	0.1565	0.1199
C_l for $D_1 = 100$ mm	0.3441	0.2062	-0.0106	-0.2062	-0.3441
C_l for $D_2 = 300$ mm	0.3422	0.2090	0.0126	-0.2083	-0.3427

3.2.2 Velocity and pressure contours, streamlines patterns

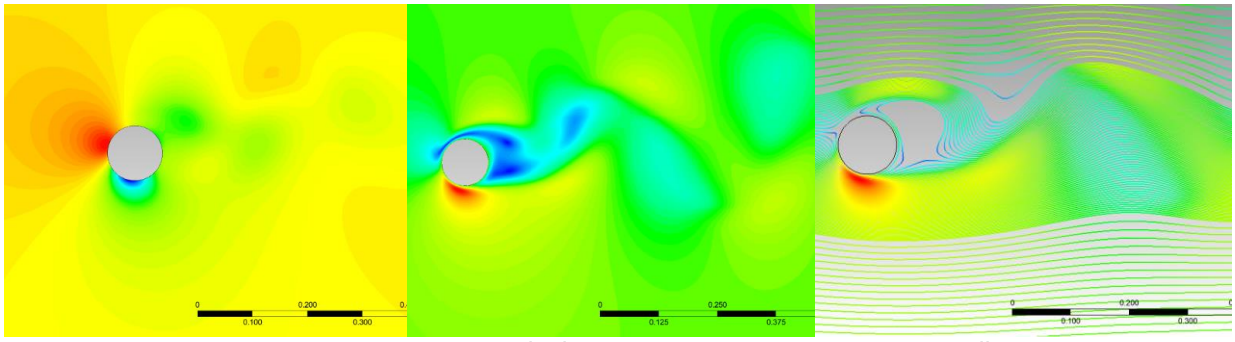
Fig. 6 and 7 demonstrate that the diameter of the cylinder has little effect on the flow behavior under a steady regime. As a result, we concentrated on varying the Reynolds number in both unsteady laminar and turbulent regimes at different alpha values in order to investigate the effect on flow behavior. The differences between unstable laminar flow at $\mathrm{Re} = 150$ and turbulent flow at $\mathrm{Re} = 1000$ are depicted in Fig. 6 and 7. While the pressure and velocity contours and streamline patterns are identical for both cylinder diameters, we studied the contours and streamlines for a $D = 100$ mm diameter cylinder to highlight the effects of CCW and CW rotation on flow behavior across a large computational domain. Our results reveal that both CCW and CW rotation can reduce pressure

distribution instabilities that occur behind the cylinder in stationary flow, and the front stagnation pressure varies based on rotation direction. The amplitude of the flow oscillation grows as the alpha parameter increases, and the oscillation goes in the direction of each alpha value. In addition, when alpha increases, the variation of flow velocity reduces, and fluid particles on the cylinder surface accelerate in the direction of the rotation parameter. As shown in the images below, the rotation parameter can alter the magnitude of flow oscillation in both CCW and CW situations and prevent pressure distribution instabilities for both Reynolds numbers.



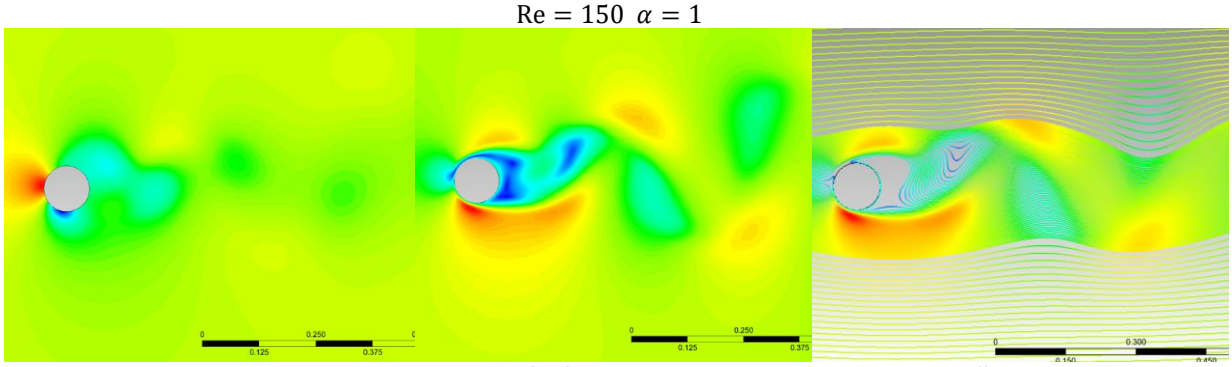
Pressure contour Velocity contour Streamlines patterns

$\mathrm{Re} = 150 \;\; \alpha = 0$



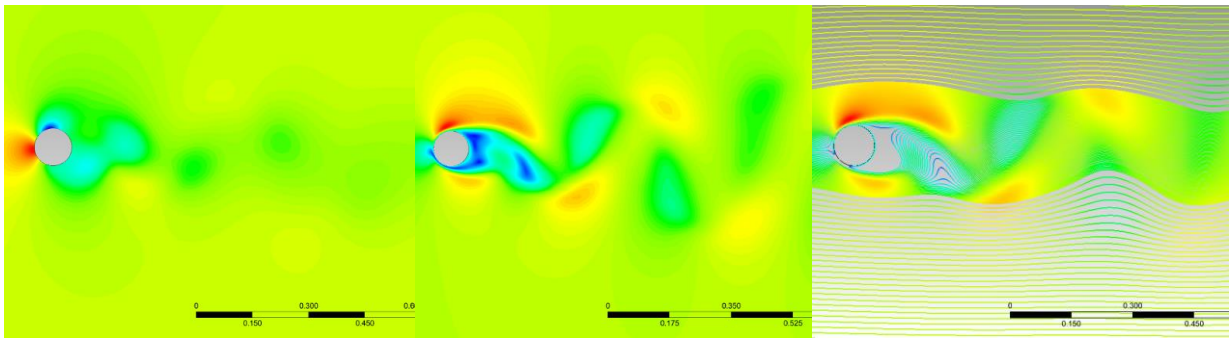
Pressure contours Velocity contours Streamlines patterns

$\mathrm{Re} = 150 \;\; \alpha = 1$



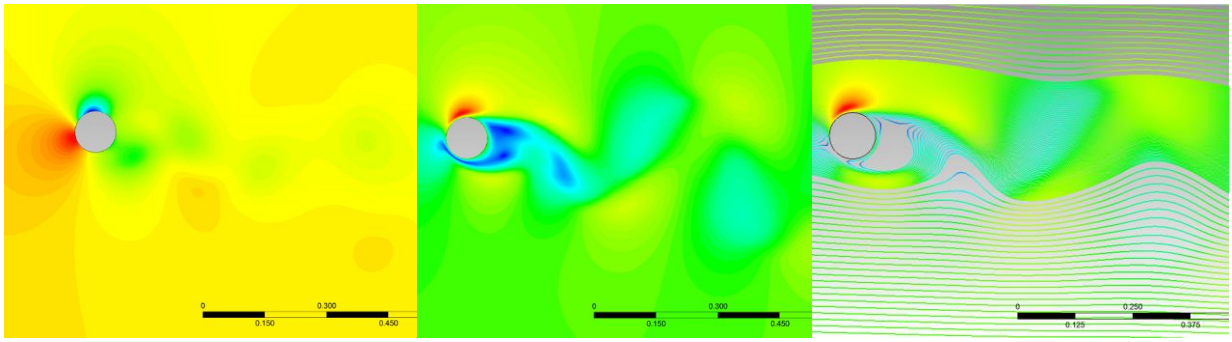
Pressure contours Velocity contours Streamlines patterns

$\mathrm{Re} = 150 \;\; \alpha = 0.5$



Pressure contours Velocity contours Streamlines patterns

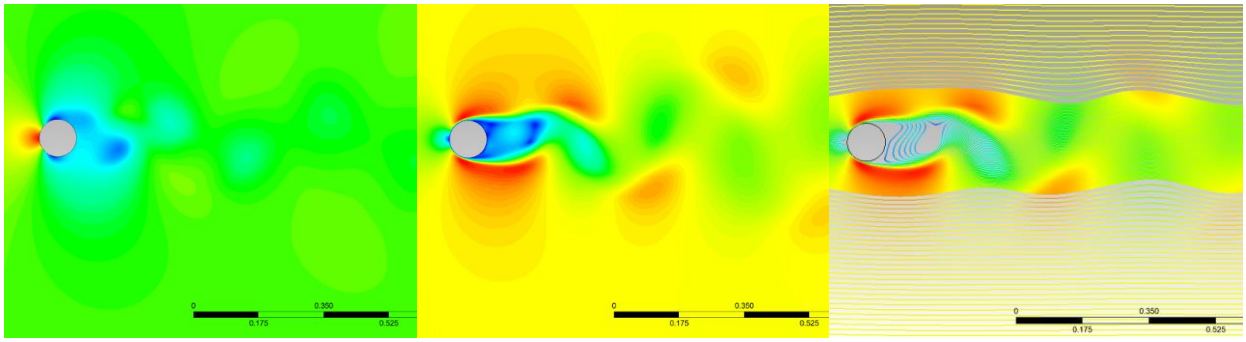
$\mathrm{Re} = 150 \;\; \alpha = -0.5$



Pressure contours Velocity contours Streamlines patterns

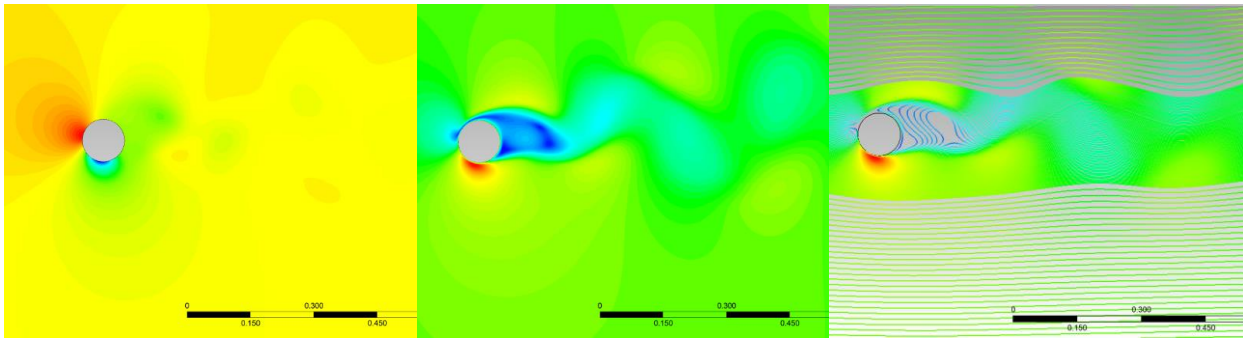
$\mathrm{Re} = 150 \;\; \alpha = -1$

Fig. 6: pressure and velocity contour, streamlines patterns $\mathrm{Re} = 150$ for $D_1 = 100$ mm.



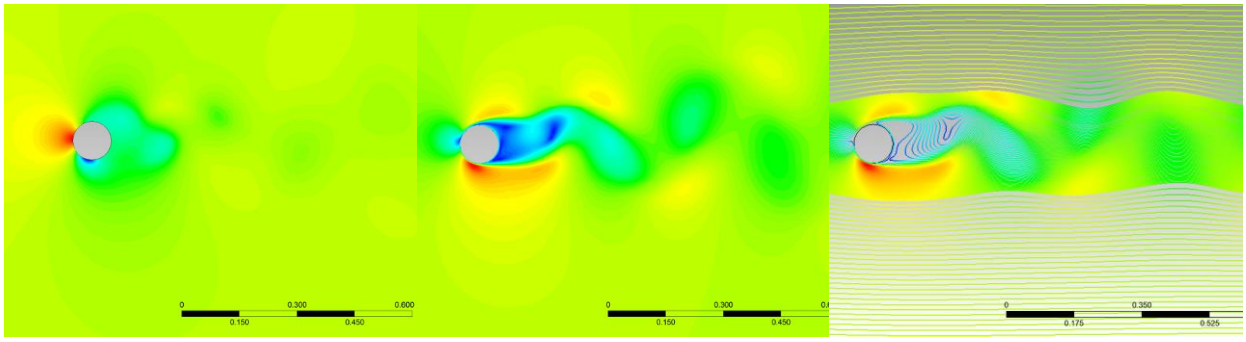
Pressure contours Velocity contours Streamlines patterns

$\mathrm{Re} = 1000 \;\; \alpha = 0$



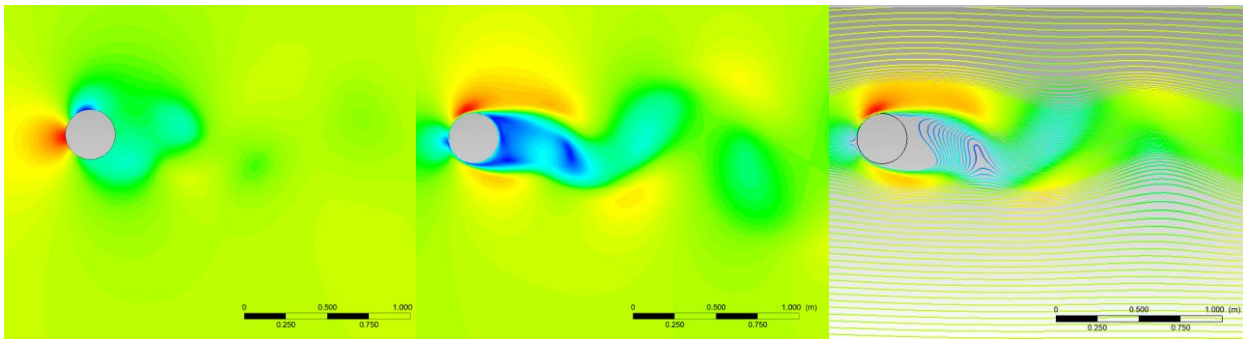
Pressure contours Velocity contours Streamlines patterns

$\mathrm{Re} = 1000 \;\; \alpha = 1$



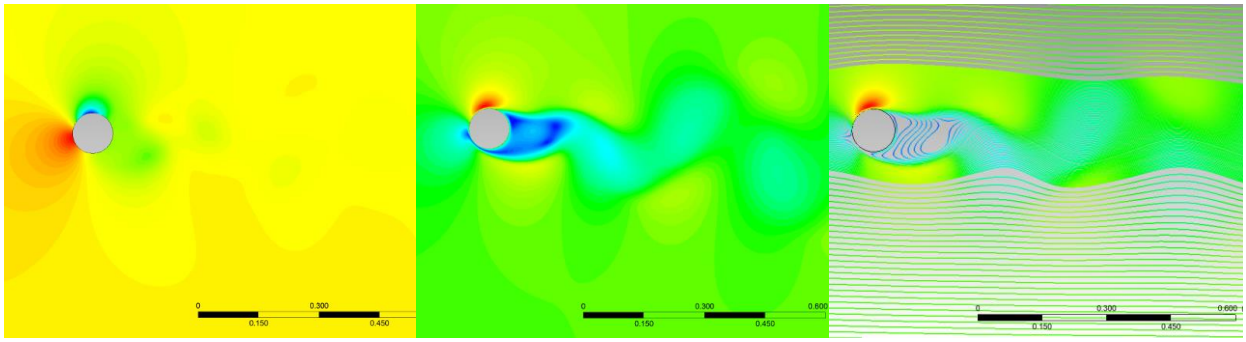
Pressure contours Velocity contours Streamlines patterns

$\mathrm{Re} = 1000 \;\; \alpha = 0.5$



Pressure contours Velocity contours Streamlines patterns

$\mathrm{Re} = 1000 \;\; \alpha = -0.5$



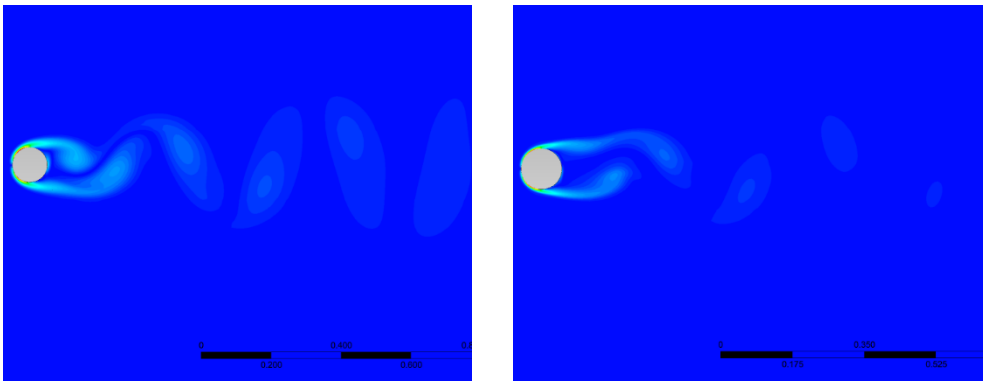
Pressure contours Velocity contours Streamlines patterns

$\mathrm{Re} = 1000 \;\; \alpha = -1$

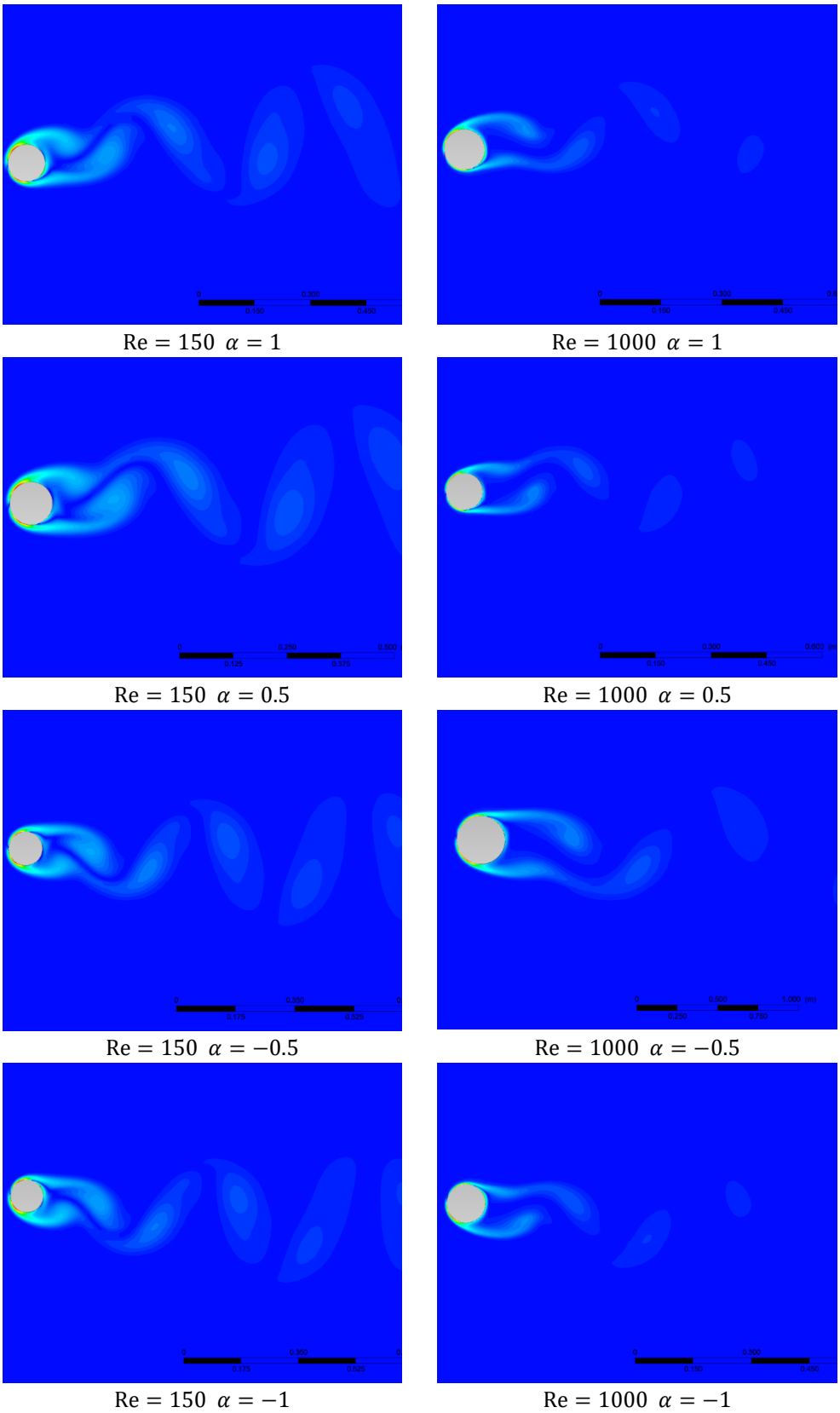
Fig. 7: pressure and velocity contour, streamlines patterns $Re = 1000$ for *D* = 100 mm.

3.2.3 Vorticity contours at $\mathbf{Re = 150}$ and $\mathbf{Re = 1000}$

Several investigations [1, 3] have demonstrated that increasing the rotation parameter can reduce vortex shedding and stabilize the flow behind a cylinder during unsteady flow by increasing the rotation parameter. In our work, we did not reach the crucial value of alpha that causes this phenomena; rather, we observed vortex shedding behavior in CCW rotation, where the rotation opposes the fluid motion, using a different technique. CCW and CW rotation have the same effect on vortex shedding in a broad computational domain and for low alpha values, where the Kármán vortex does not evaporate at a Reynolds Re = 150. Around Re = 1000 the stationary Kármán vortex street begins to shrink due to the influence of the turbulent regime, Fig. 8. At an $\alpha = 0.5$, vortex shedding resembles the stationary case in which the vortex oscillates along the horizontal centerline. At $\alpha = 1$, the shape of vortex shedding does not change; only the oscillation bends upwards and downwards in the direction of rotation. In a vast fluid domain, CCW rotation has no effect on vortex shedding in the wake. As shown by a prior study [11], the only way to prevent vortex shedding is at a critical alpha value of α = 1.4.



$\mathrm{Re} = 150 \;\; \alpha = 0$ $\mathrm{Re} = 1000 \;\; \alpha = 0$



$\mathrm{Re} = 150 \;\; \alpha = 1$ $\mathrm{Re} = 1000 \;\; \alpha = 1$

$\mathrm{Re} = 150 \;\; \alpha = 0.5$ $\mathrm{Re} = 1000 \;\; \alpha = 0.5$

$\mathrm{Re} = 150 \;\; \alpha = -0.5$ $\mathrm{Re} = 1000 \;\; \alpha = -0.5$

$\mathrm{Re} = 150 \;\; \alpha = -1$ $\mathrm{Re} = 1000 \;\; \alpha = -1$

Fig. 8: Vorticity contours.

4 Conclusion

In steady and unsteady flow regimes, the influence of cylinder diameter and rotation rate parameters on the behavior of the flow at different Reynolds numbers was investigated. According to

current studies, drag and lift coefficients, pressure and velocity contours, and streamline patterns have all been analyzed. In all cases, the values of drag and lift were strongly related to changes in Reynolds number and rotation rate parameter, as shown in tables 1, 2, 4, 5, 6, and 7. However, in the steady case at Re = 40, we observed a slight difference in the results of drag and lift coefficients affected by the change in cylinder diameter. The values of drag and lift changed as the Reynolds number increased, which is consistent with the findings of the scientific literature [14, 22]. Numerous investigations have demonstrated that the rotation of a cylinder in a fluid flow decreases and increases the values of drag and lift, respectively. The drag and lift findings in CCW rotation were comparable, with the exception of the situation presented in Table 3. The main distinction between CW and CCW rotation was evident in the stagnation point of the pressure and velocity contours, which altered with the direction of rotation. At low Reynolds numbers, both CCW and CW rotation lost symmetry. Vortex shedding oscillates in accordance with the rotational direction. Both CCW and CW have altered the pressure distribution around and along the wake in an unstable zone, where the rotation inhibited the instabilities caused by the cylinders. Attempts to examine the effect of CWW or CW rotation on a circular cylinder in a substantial fluid domain will yield comparable results for both rotations. These findings imply that rotation can influence the velocity and acceleration of fluid particles on the cylinder's surface, which may have significant consequences for a variety of engineering applications. This work illustrates the complicated interaction between rotation and flow behavior around a cylinder in a broad computational domain and argues that more research is required to properly comprehend and exploit the potential advantages of rotation in a variety of engineering applications.

References

[1] ASHOURI, A. - IZADPANAH, E. - HEKMAT, M. H. - AMINI, Y.: Numerical investigation on two-degree-of-freedom vortex-induced vibration of a circular cylinder in power-law fluids. Journal of Non-Newtonian Fluid Mechanics, 292, 2021, 104535.
[2] BADR, H. M. - COUTANCEAU, M. - DENNIS, S. C. - MENARD, C.: Unsteady flow past a rotating circular cylinder at Reynolds numbers 103 and 104. Journal of Fluid Mechanics, 1990, 459-484.
[3] BEARMAN, P. W.: Understanding and predicting vortex-induced vibrations. Journal of Fluid Mechanics, 634, 2009, pp. 1-4.
[4] BEHR, M. - HASTREITER, D. - MITTAL, S. - TEZDUYAR, T. E.: Incompressible flow past a circular cylinder: dependence of the computed flow field on the location of the lateral boundaries. Computer Methods in Applied Mechanics and Engineering, 123(1-4), 1995, pp. 309-316.
[5] CANBOLAT, G. - YILDIZELI, A. - KÖSE, H. A. - ÇADIRCI, S.: Numerical Investigation of Transitional Flow over a Flat Plate under Constant Heat Fluxes. Academic Perspective Procedia, 1(1), 2018, p. 187-195.
[6] COUTANCEAU, M. - MENARD, C.: Influence of rotation on the near-wake development behind an impulsively started circular cylinder. Journal of Fluid Mechanics, 158, 1985, pp. 399-446.
[7] DENNIS, S. C. - CHANG, G. Z.: Numerical solutions for steady flow past a circular cylinder at Reynolds numbers up to 100. Journal of Fluid Mechanics, 42(3), 1970, pp. 471-489.
[8] FORNBERG, B.: A numerical study of steady viscous flow past a circular cylinder. Journal of Fluid Mechanics, 98(4), 1980, pp. 819-855.
[9] GIORIA, R. S. - MENEGHIN, J. R. - ARANHA, J. A. - BARBEIRO, I. C. - CARMO, B. S.: Effect of the domain spanwise periodic length on the flow around a circular cylinder. Journal of fluids and structures, 27(5-6), 2011, pp. 792-797.
[10] INGHAM, D. B.: Steady flow past a rotating cylinder. Computers & Fluids, 11(4), 1983, 351-366.
[11] KANG, S. - CHOI, H. - LEE, S.: Laminar flow past a rotating circular cylinder. Physics of Fluids, 11(11), 1999, pp. 3312-3321.
[12] LAUSOVÁ, L. - KOLOŠ, I. - MICHALCOVÁ, V.: Comparison of 2D Grid Simulations for Flow Past Cylinder at High Reynolds Numbers. Civil and Environmental Engineering, 15(1), 2019, pp. 70-78, doi: https://doi.org/10.2478/cee-2019-0010.
[13] PRANDTL, L.: The Magnus effect and wind-powered ships. Naturwissenschaften, 13(6), 1925, pp. 93-108.
[14] RAHMAN, M. - KARIM, M. - ALIM, A.: Numerical investigation of unsteady flow past a circular cylinder using 2-D finite volume method. Journal of Naval Architecture and Marine Engineering, 4(1), 2007, pp. 27-42.
[15] SALEHI, M. A. - MAZAHERI, S. - KAZEMINEZHAD, M. H.: Study of Flow Characteristics around a Near-Wall Circulair Cylinder Subjected to a Steady Cross-Flow. International journal of coastal & offshore engineering, 1(4), 2018, pp. 45-55.

[16] SARKAR, S. - SARKAR, S.: Simulation of vortex dynamics in a cylinder wake by the Immersed Boundary. Progress in Computational Fluid Dynamics, 10(3), 2010, pp. 129-145.
[17] SREENIVASAN, K. R. - STRYKOWSKI, P. J. - OLINGER, D. J.: Hopf bifurcation, Landau equation, and vortex shedding behind circular cylinders. Forum on unsteady flow separation,(p. 1-13, 1987, New York: ASME.
[18] SUCKER, D. - BRAUER, H.: Investigation of the flow around transverse cylinders (Fluiddynamik bei quer angeströmten Zylindern). Wärme-und Stoffübertragung, 8, 1975, ppp. 149-158.
[19] TEZDUYAR, T. E., & SHIH, R. (1991). Numerical experiments on downstream boundary of flow past cylinder. Journal of engineering mechanics, 117(4), pp. 854-871.
[20] TOKUMARU, P. T. - DIMOTAKIS, P. E.: Rotary oscillation control of a cylinder wake. Journal of Fluid Mechanics, 224, 1991, pp. 77-90.
[21] TOKUMARU, P. T. - DIMOTAKIS, P. E.: The lift of a cylinder executing rotary motions in a uniform flow. Journal of fluid mechanics, 255, 1993, pp. 1-10.
[22] TRITTON, D. J.: Experiments on the flow past a circular cylinder at low Reynolds numbers. Journal of Fluid Mechanics, 4, 1959, pp. 547-567.